# Non-Turing stationary patterns in flow-distributed oscillators with general diffusion and flow rates

Razvan A. Satnoianu[1] and Michael Menzinger[2]
[1]*Centre for Mathematical Biology, Mathematical Institute, University of Oxford, Oxford OX1 3LB, United Kingdom*
[2]*Department of Chemistry, University of Toronto, Toronto, Ontario, Canada M5S 3H6*
(Received 15 October 1999)

An analytical prediction [P. Andresen *et al.*, Phys. Rev. E **60**, 297 (1999)] and its experimental confirmation [M. Kaern *et al.*, Phys. Rev. E **60**, 3471 (1999)] establish a mechanism for forming stationary, space-periodic structures in a reactive flow (reaction-diffusion-convection system) with equal diffusion and flow rates. In this paper we generalize the analysis to systems with unequal diffusion and flow rates. Interestingly, stationary waves also exist outside the oscillatory Hopf domain of the batch system—hence the parameter space in which these structures exist is bigger than that initially predicted [P. Andresen *et al.*, Phys. Rev. E. **60**, 297 (1999)] (for equal diffusion and flow rates). On the other hand, we find that these stationary waves exist only for parameter values outside of and up to the Turing regime. We clarify the nature of the instability in terms of a boundary-forcing problem, whereby a time-periodic pattern is carried over the whole domain by the flow while the phase is fixed at the inflow boundary.

PACS number(s): 82.20.−w

## I. INTRODUCTION

Andresen *et al.* [1] proposed an alternative spatial instability mechanism that gives rise to stationary, space-periodic patterns in a time-oscillating reaction-diffusion-convection system with equal diffusion and flow rates through the constant forcing at the inflow boundary of the flow domain (see also the earlier contribution [2]). This mechanism is interesting since it differs fundamentally from the Turing [4] and differential flow instabilities (DIFI) [3], which require differential transport of the key species, and since the conditions for the alternative instability may be readily realized in chemical flow reactors, using active media in the oscillatory (Hopf) domain. This prediction was confirmed experimentally by Kaern and Menzinger [5]. From their results it is clear that the patterns arise by a mechanism that is essentially kinematic. Accordingly, the flow carries temporal oscillations into space, while the oscillation phase is locked at the inflow boundary through a constant boundary condition. Therefore we refer to these stationary structures as flow-distributed oscillations (FDO).

In this work we generalize the above results to the case of a reaction-diffusion-convection system with differential transport, i.e., with different diffusion and flow rates. To distinguish the resulting waves (for this more general case) from the FDO waves, we refer to them here as flow-distributed structures or FDS. The analysis provides the boundary of the FDS instability in the parameter domain and clarifies its relation to Turing and DIFI patterns. We analyze how this instability connects with the Turing and DIFI domains and discuss the interface with, and difference from, the two classical, differential transport-induced instability mechanisms. This paper sheds light on how the region, where stationary Turing patterns are observed in the absence of a bulk flow, may be extended by the presence of a flow. We find that an unstable (Hopf) reference state is not necessary for FDS to occur, and that their domain extends into the region where the reference state is stable. Our analytical results confirm the kinematic interpretation [5] that the FDO instability is being driven by boundary forcing that freezes the temporal oscillation phase of the species traveling along the flow domain until the other boundary is encountered.

## II. A REACTION-DIFFUSION-CONVECTION SYSTEM WITH UNEQUAL DIFFUSION AND FLOW RATES: AN IONIC CHEMICAL SYSTEM WITH CUBIC AUTOCATALYTIC STEP

We generalize the problem considered in [1] by employing a model for a differential-flow reactor based on applying an electric field to a reacting medium with an ionic version of cubic autocatalator (or Gray-Scott) kinetics [6]. The differential flow (or migration) of the reacting species arises since substrate $A^+$ and autocatalyst $B^+$ have different drift velocities due to their different diffusion coefficients. By using the cubic autocatalator model (as opposed to the Brusselator model in [1]) it simplifies considerably the details of the subsequent calculations while still preserving all the features of the general case.

The model assumes that we have a precursor $P^+$ present in excess. To maintain electroneutrality we also require a further species $Q^-$ to be present in the reactor at a concentration similar to that of $P^+$, though this species does not take part in the reaction. We assume that $P^+$ decays at a constant rate to form the substrate $A^+$ via

$$P^+ \rightarrow A^+, \quad \text{rate} = k_0 p_0, \tag{2.1}$$

where $p_0$ is the initial concentration of the reservoir species $P^+$. The substrate $A^+$ and autocatalyst $B^+$ subsequently react according to the scheme

$$A^+ + 2B^+ \rightarrow 3B^+, \quad \text{rate} = k_1 a b^2, \tag{2.2}$$

$$B^+ \rightarrow C^+, \quad \text{rate} = k_2 b, \tag{2.3}$$

 

where the $k_i$ are constants and $a$, $b$ are the concentrations of $A^+$ and $B^+$. The nonionic version of this scheme is fully described in [7], where a justification for the pool chemical approximation, which allows step (2.1) to proceed at a constant rate, is given.

With $P^+$ and $C^+$ present in excess, so that reactions (2.2) and (2.3) make only a small net contribution to the overall ionic balance, we can invoke the constant field approximation used extensively in previous models. A formal justification for this approximation is given in [8]. We take the reactor to be such that transverse variations in concentration can be neglected, and it is sufficiently long for end effects to be negligible [5]. This leads to the dimensionless reactor model (see [6] for the derivation of these equations and the influence of the electric field in their form)

$$\frac{\partial a}{\partial t}=\delta\frac{\partial^2 a}{\partial x^2}-\delta\phi\frac{\partial a}{\partial x}+\mu-ab^2, \tag{2.4}$$

$$\frac{\partial b}{\partial t}=\frac{\partial^2 b}{\partial x^2}-\phi\frac{\partial b}{\partial x}+ab^2-b, \tag{2.5}$$

where $a$, $b$, $t$, and $x$ are the dimensionless concentrations, time, and distance along the reactor with $t>0$ and $0<x<\infty$. Here $\delta=D_A/D_B$ is the ratio of diffusion coefficients of substrate $A^+$ and autocatalyst $B^+$, respectively, and $\phi$ is the dimensionless drift velocity of $B^+$, which we use as the bifurcation parameter. Since $\delta$ couples the differential-diffusion and flow [through the $\delta\phi$ term in Eq. (2.4)] it is also called the differential transport ratio. Without any loss of generality we assume that $\phi>0$. On putting $\delta=0$ in Eqs. (2.4) and (2.5) we recover the model discussed in Satnoianu *et al.* [9] and Merkin *et al.* [10].

The kinetic system, (2.4) and (2.5), has a (spatially uniform) steady state $S=(a,b)=(\mu^{-1},\mu)$ that is stable for $\mu>1$ and undergoes a supercritical Hopf bifurcation at $\mu=1$. This leads to stable limit cycles in the interval $\mu_0<\mu<1$ ($\mu_0\cong 0.9003$). For $\mu<\mu_0$, the kinetic system does not have a long-time steady state with $a\sim\mu t$, $b\to 0$ as $t\to\infty$. We assume that initially the system is in its spatially uniform reference state $S$, taking

$$a=\mu^{-1},\quad b=\mu\quad \text{at } t=0,\quad 0<x<\infty. \tag{2.6}$$

A small, constant perturbation in the autocatalyst concentration is made to this state at the inlet ($x=0$) for all $t>0$:

$$b(0,t)=\mu+b_0,\quad 0<|b_0|\ll 1, \tag{2.7}$$

where $b_0$ is a constant for all $t>0$. We take conditions to be uniform at infinity so that

$$\frac{\partial a}{\partial x}\to 0,\quad \frac{\partial b}{\partial x}\to 0,\quad \text{as } x\to\infty,\quad t>0, \tag{2.8}$$

and keep the reactant concentration at its steady state value at $x=0$,

$$a(0,t)=\mu^{-1}\quad \text{for all } t>0. \tag{2.9}$$

Andersen *et al.* [1] have considered the system in the Hopf domain $\mu_0<\mu<1$ where the steady state $S$ is unstable. However, we do not restrict ourselves to the Hopf domain and will leave $\mu$ unconstrained in order to deduce all possible regimes that give rise to stationary, space-periodic structures. Our goal is to study the effect of the applied electric field upon the steady state $S$, and if $S$ is unstable toward small perturbations (2.7), to determine what kind of pattern emerges. To do so we perform a linear stability analysis.

## III. LINEAR STABILITY ANALYSIS

System (2.4)–(2.9) constitutes a closed initial-value problem. Its main feature is the boundary perturbation at the upstream boundary $x=0$ that persists for all $t>0$ [Eq. (2.7)]. This is a so-called *constant boundary-forcing problem*. A similar problem was already analyzed in [11] for the system (2.4) and (2.5) but with $\delta=0$ and when a periodic temporal signal is applied at the boundary in the autocatalyst concentration. Nevertheless, the methods used in [11] are general and as such they can be applied to the present problem.

To examine the stability of the steady state $S$ to small perturbations we put

$$a=\mu^{-1}+A,\quad b=\mu+B, \tag{3.1}$$

where $A\ll a$, $B\ll b$ are small. Substituting Eq. (3.1) into Eqs. (2.4) and (2.5) gives, after linearizing,

$$\frac{\partial A}{\partial t}=\delta\frac{\partial^2 A}{\partial x^2}-\delta\phi\frac{\partial A}{\partial x}-\mu^2 A-2B, \tag{3.2}$$

$$\frac{\partial B}{\partial t}=\frac{\partial^2 B}{\partial x^2}-\phi\frac{\partial B}{\partial x}+\mu^2 A+B. \tag{3.3}$$

We express the solution of Eqs. (3.2) and (3.3) in terms of Fourier transforms in space as

$$(A,B)=\frac{1}{2\pi}\int_{-\infty}^{\infty}(A_0(\omega),B_0(\omega))e^{i\omega+k(\omega)x}d\omega. \tag{3.4}$$

The functions $A_0(\omega),B_0(\omega)$ depend on the form of the initial data. In our case we assume that the perturbation is applied at the inflow boundary $x=0$ for a long but finite time. This allows us to take initial data with time-compact support for which the solutions to Eq. (3.4) are analytic functions in the complex $\omega$ plane.

Before discussing the dispersion relation for problem (3.1)–(3.4), it is instructive to recall some facts about the stability of the steady state $S$ when the system is subject to *spatially localized perturbations* [12,6]. In this case relation (3.4) is modified to

$$(A,B)=\frac{1}{2\pi}\int_{-\infty}^{\infty}(A_0(k),B_0(k))e^{\omega(k)t+ikx}dk, \tag{3.5}$$

where $\omega$ satisfies the dispersion relation

$$\omega^2+[(\delta+1)k^2+i(\delta+1)\phi k+\mu^2-1]\omega+\delta k^4+2i\delta\phi k^3 +(\mu^2-\delta-\delta\phi^2)k^2+i\phi(\mu^2-\delta)k+\mu^2=0. \tag{3.6}$$

Note that Eq. (3.6) reduces to the dispersion relation derived in [12] for the case (DIFI) arising from a totally immobilized substrate $A^+$ if we put $\delta=0$. It also gives the dispersion

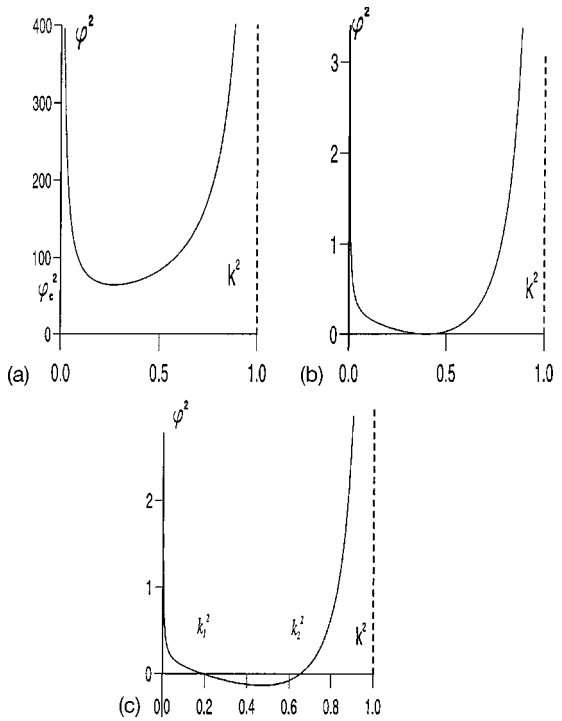


FIG. 1. A typical neutral curve $\phi_*$, defined in Eq. (3.7), for the three different cases: (a) $\mu^2>(3-2\sqrt{2})\delta$, (b) $\mu^2=(3-2\sqrt{2})\delta$, and (c) $\mu^2<(3-2\sqrt{2})\delta$, respectively.

relation for *Turing instability* [7] if we set $\phi=0$. From Eq. (3.6) we can derive the DIFI neutral curves; i.e., those curves in $\phi$-$k$ space on which $\mathrm{Re}(\omega)=0$. After a little calculation we find that these are given by

$$\phi_*^2=\frac{[\delta k^4+(\mu^2-\delta)k^2+\mu^2][(1+\delta)k^2+\mu^2-1]^2}{(\delta-1)^2(1-k^2)(\mu^2+\delta k^2)k^2},$$

$$\text{for } 0<k<1 \tag{3.7}$$

for $\delta\neq 1$. When $\delta=1$, i.e., in the absence of a differential transport, $\mathrm{Re}(\omega)<0$ for all values of $\phi$ and $\mu>1$ (in fact, $\inf\phi_*=\infty$). A necessary condition for Eq. (3.7) to hold is that $0<k<1$ with the curve having vertical asymptotes at $k=0$ and $k=1$. The form of the neutral curve then depends on the sign of the term

$$T\equiv\delta k^4+(\mu^2-\delta)k^2+\mu^2. \tag{3.8}$$

The curve $T=0$ gives the neutral curve for *Turing instabilities* in the absence of an electric field (differential flow) [7], with the condition that $\mu^2<(3-2\sqrt{2})\delta$ being needed to have a finite range of wave numbers $k$ over which the steady state $S$ is unstable to small perturbations. When $\mu>1$, a *necessary condition for Turing instability* is therefore that $\delta>(3+2\sqrt{2})\mu^2$.

When $T>0$ [i.e., $\mu^2>(3-2\sqrt{2})\delta$] the expression on the right-hand side of Eq. (3.7) is positive for all $k$ on $0<k<1$ and the neutral curve $\phi_*=\phi(k,\delta,\mu)$ has a minimum at a nonzero value of $\phi_*=\phi_*^c(\mu,\delta)>0$. A typical neutral curve for this case is shown in Fig. 1(a).

When $\mu^2=(3-2\sqrt{2})\delta$, $T=0$ at $k^2=\sqrt{2}-1$ for all $\delta$, and the neutral curve touches the $\phi=0$ axis at this value of $k$. This case is illustrated in Fig. 1(b).

When $\mu^2<(3-2\sqrt{2})\delta$, $T=0$ at $k_{1,2}$ where

$$k_{1,2}=\tfrac{1}{2}(1-Y\mp\sqrt{1-6Y+Y^2}),\quad Y=\frac{\mu^2}{\delta}<(3-2\sqrt{2})\delta, \tag{3.9}$$

and $0<k_1^2<k_2^2<1$. In this case the instability arises from both *Turing and DIFI mechanisms*, and the curve on which $\mathrm{Re}(\omega)=0$ consists of two sections, namely, the values of $\phi$ given by expression (3.7) for $0<k\leqslant k_1$ and $k_2\leqslant k<1$ and $\phi=0$ for $k_1\leqslant k\leqslant k_2$. This case is illustrated in Fig. 1(c).

From this discussion we conclude that there are ranges of wave number $k$ over which $\mathrm{Re}(\omega)>0$ [for $\phi\geqslant\phi_c>0$ with $\mu^2>(3-2\sqrt{2})\delta$ and for $\phi>0$ with $\mu^2\leqslant(3-2\sqrt{2})\delta$] where the spatially uniform state $S$ is unstable to small perturbations. No other instabilities from $S$ are possible for $\mu>1$.

Now we return to the original problem (3.1)–(3.4). Using Eq. (3.4) in Eqs. (3.2) and (3.3), a brief calculation gives the dispersion relation

$$-\omega^2+i(-(\delta+1)k^2+(\delta+1)\phi k+\mu^2-1)\omega+\delta k^4-2\delta\phi k^3$$
$$-(\mu^2-\delta-\delta\phi^2)k^2+\phi(\mu^2-\delta)k+\mu^2=0. \tag{3.10}$$

Since we are interested in stationary bifurcating solutions, we set $\omega=0$ and obtain

$$R\equiv\delta k^4-2\delta\phi k^3+(\delta+\delta\phi^2-\mu^2)k^2+\phi(\mu^2-\delta)k+\mu^2=0. \tag{3.11}$$

Equation (3.11) may have a complex solution $k$. Solutions that bifurcate to space-periodic structures will have purely imaginary wave numbers $k_c=iz_c$, $z_c>0$. A short calculation reveals that

$$z_c=\sqrt{\frac{\delta-\mu^2}{2\delta}}. \tag{3.12}$$

Note that this bifurcation can only exist when $\delta>\mu^2$. Putting this value of $k$ in Eq. (3.11) gives the *neutral curve of the boundary-forcing problem*, i.e., the curve $\phi^*=\phi(\delta,\mu)$, which corresponds to the *bifurcation to stationary (FDS) solutions*

$$\phi^{*2}=-\frac{1}{2}\frac{\delta^2-6\delta\mu^2+\mu^4}{\delta(\delta-\mu^2)} \tag{3.13}$$

for $\delta\neq 0$. We have that $\phi^*\to\infty$ as $\delta\to\mu^2$ (from above) and $\phi^*\to 0$ as $\delta\to(3+2\sqrt{2})\mu^2$ (from below), with $\phi^*$ having a decreasing, convex shape for all intermediate values $\mu^2<\delta<(3+2\sqrt{2})\mu^2$. Since the right-hand side of Eq. (3.13) must be positive it follows, via Eq. (3.12), that Eq. (3.13) can only exist for

$$\mu^2<\delta<(3+2\sqrt{2})\mu^2=\delta_T. \tag{3.14}$$

From our discussion following Eq. (3.8), $\delta_T$ is the boundary of the Turing domain. In particular, we see that no bifurcation to stationary FDS is possible when $\delta=1$ and $\mu\geqslant 1$, i.e., outside the batch mode limit cycle (Hopf) domain, in accord with [1,5]. However, FDS may arise for any $\delta\neq 1$ for a certain range of values of $\mu>1$. The FDS instability thus extends to both sides of the Hopf domain $\mu_0<\mu\leqslant 1$ of

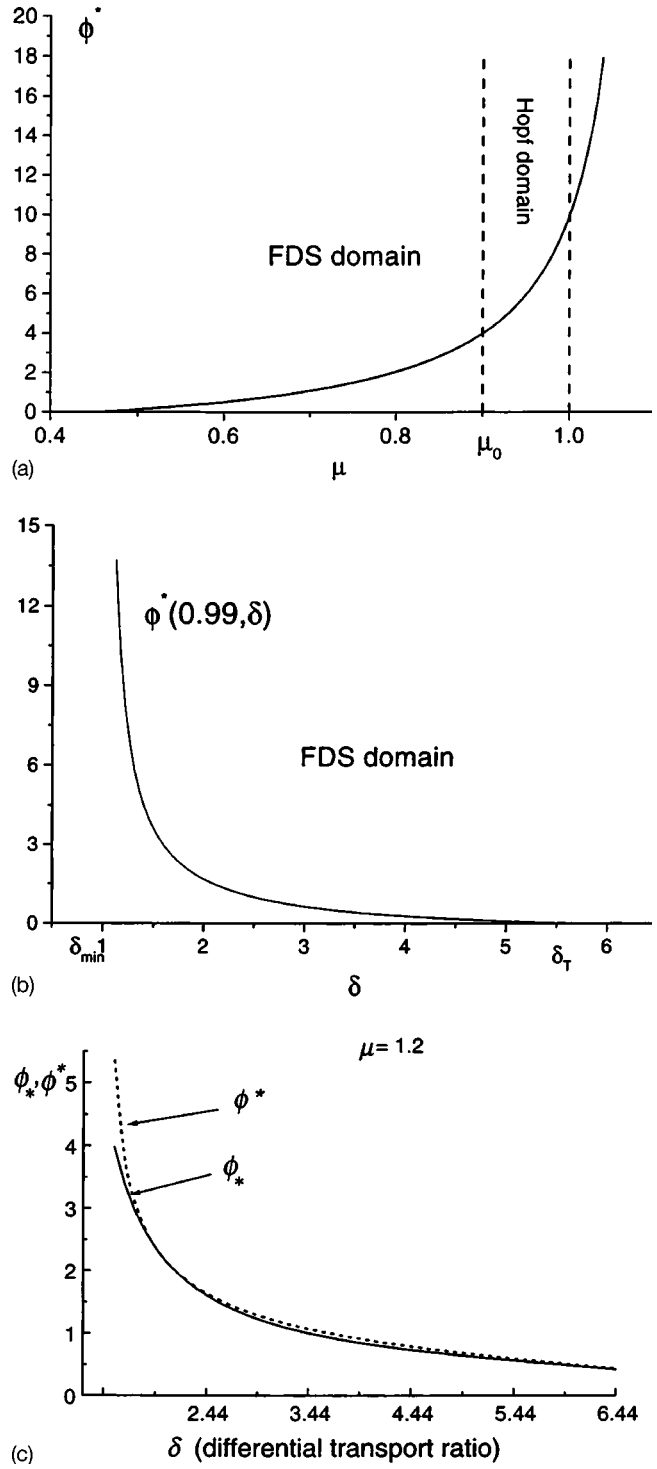


FIG. 2. (a). Plot of the neutral curve $\phi^*$ given in Eq. (3.13) for $\delta=1.2$ and $\sqrt{(3-2\sqrt{2})\,\delta}=0.453<\mu<\sqrt{\delta}=1.09$. (b). Plot of the neutral curve $\phi^*$ given in Eq. (3.13) for $\mu=0.99$ and $\mu^2=0.9801=\delta_{\min}<\delta<\delta_T=(3+2\sqrt{2})\mu^2=5.71$. (c). A comparison between the values of neutral curve $\phi^*$ (3.13) to those of the minimum of the neutral curve for $\phi_*$ (DIFI) given in Eq. (3.7) for $\mu>1$. Here for the case $\mu=1.2$.

the homogeneous system; i.e., stationary FDS solutions arise in the nonoscillating $1<\mu$ domain as well as in the unstable $\mu<\mu_0$ domain of the kinetic system (2.1)–(2.3).

A plot of the neutral curve $\phi^*=\phi^*(1.2,\mu)$ (for $\delta=1.2$) is given in Fig. 2(a), and a plot of the curve $\phi^*=\phi^*(\delta,0.99)$ (for $\mu=0.99$) is given in Fig. 2(b). Figure 2(a) demonstrates that the regime of stationary FDS solutions extends well beyond the unstable Hopf domain ($\mu_0\approx0.9003<\mu\leqslant1$) of the homogeneous batch system, both into the stable domain ($\mu>1$) and into the unstable domain ($\mu<\mu_0$), which lacks an attractor in the batch but which may be stabilized by a flow to give FDS solutions.

It is instructive to compare the values of the FDS neutral curve (3.13), $\phi^*$, with those of the minimum of the DIFI neutral curve for $\phi_*$ given by Eq. (3.7) for $\mu>1$. This is shown in Fig. 2(c) for the value $\mu=1.2$. We see that the neutral curve for stationary FDS solutions (denoted by $\phi^*$ in this figure) always lies above the corresponding value of the minimum of the neutral curve of the DIFI problem (which incidentally corresponds [11] to the minimum of the DIFI forcing problem). This shows that the dynamic regime is set by the DIFI instability, but unlike the DIFI (where there are always traveling waves born from the primary DIFI bifurcation [12]), we have here stationary waves. Note also that the two curves are tangent at some intermediate value of $\delta$ (here $\delta\approx2.0$) and that they converge again asymptotically as $\delta\rightarrow\infty$ (even if the curves are only defined for $\delta\leqslant\delta_T$). Furthermore, we have repeated these calculations for a range of values of $\mu$ and found the same conclusion all the time, implying that this is a general feature. It is clear that the DIFI convective regime established for our system in [6] (see also [13,14]) is a necessary requirement for the stationary wave, FDS instability to set in, since this convective mechanism is the physical way by which the initial boundary instability is transported all the way into the spatial domain.

From the above we deduce two important conclusions. First, this instability to space-periodic patterns is not restricted to $\delta=1$ (equal diffusion and implicitly flow rates), but in fact it does hold for a whole range of values [as given by Eq. (3.14)] bounded from above by the Turing boundary $\delta=\delta_T$. Second, there is no restriction on $\mu$ that requires the system to lie within the Hopf domain, as presented in [1]. This result is by far richer than what one could anticipate. This type of structure has in fact been observed experimentally outside the basin of attraction of the batch mode limit cycle [15].

## IV. NUMERICAL EXPLORATIONS

The above analysis was performed for an unbounded one-dimensional domain. The reason for this is that we were interested in the self-organization of the system for pattern formation in the absence of the boundary at the outlet. Nevertheless, in the numerical simulations to be presented below we had to impose boundary conditions at the outlet. The effect of this is to produce an imperfect FDS bifurcation (i.e., the critical FDS-flow velocity is perturbed with some small, negligible value if the simulations are run for a sufficiently long domain and the boundary condition does not force the system too much). We found that the appropriate conditions to impose are either of the zero flux or free boundary type (i.e., the second spatial derivative equals zero). The quantitative assessment of the influence of these boundary conditions used in the simulations has already been analyzed in great detail for the differential-flow system of this type in [12], so there is no need to redo this here.

We begin our discussion by analyzing the mechanism for wavelength selection to stationary, space-periodic FDS patterns. To do so, note that from Eqs. (3.11) and (3.12) the wave number at criticality is purely imaginary with

$$k_c = iz_c, \quad z_c = \sqrt{\frac{\delta-\mu^2}{2\delta}}. \tag{4.1}$$

On using Eq. (3.4), we see that the wave number (4.1) gives the most unstable ''mode,'' predicting the wavelength at criticality as

$$\lambda_c = \frac{2\pi}{z_c} = 2\pi\sqrt{\frac{2\delta}{\delta-\mu^2}}. \tag{4.2}$$

A plot of the analytical wavelength predicted from Eq. (4.2) is shown in Fig. 3(a) for the case $\mu=0.99$ and for $\mu^2=0.9801<\delta<(3+2\sqrt{2})\mu^2=5.7124\ldots$. It is easy to see that $\lambda_c$ is a decreasing function of $\delta$ (for given $\mu$) having a horizontal asymptote $\lambda_c=2\sqrt{2}\pi$ as $\delta\to\infty$.

We verified this prediction by solving the initial-value problem (2.4)–(2.9) numerically. We employed [6,12] an implicit Crank-Nicholson finite-difference scheme with the algebraic systems of equations resulting from the discretization then being solved by Newton-Raphson iteration. The method has been successfully used for a great number of reaction-diffusion-convection problems (see references in [6,12]). We performed simulations for quite a large set of parameter values but shall review here only the most generic behavior. For the simulations presented below, typical values for $b_0$ were $\pm0.1$, $\pm0.2$.

Results for $\mu=0.99$ are shown in Figs. 3(b) and 3(c) for the cases $\delta=1.2$ and $\delta=2.0$. For $\delta=1.2$ we have $\phi_c=2.98$ [from Eq. (3.13)] giving $\lambda(analytic)=20.822$. The numerical value found is $\lambda(numeric)=20.9$. For $\delta=2.0$ we have $\phi_c=1.291$ giving $\lambda(analytic)=12.442$ and $\lambda(numeric)=12.45$. We can see the decrease in the wavelength. For all the other numerically computed values the results agreed well (within the numerical accuracy of the code) with the analytical counterparts (4.2). Remarkable is the transient behavior in the autocatalyst concentration $b$ seen in Fig. 3(c), which is reminiscent of the dynamical competition between two processes, namely, the Hopf oscillatory instability of the stationary state and also the instability due to the forcing problem (stationary-periodic wave instability). The result seen here is generic for the behavior seen in all the solutions when $\delta$ was increased from 1.

We also explored the behavior of the system when $\phi$ was set sufficiently well away from the critical value (3.13). This is illustrated in Figs. 4(a) and 4(b) for $\mu=0.99$, $\delta=1.0$, and $\phi=11.0$ and 30.0, respectively. For $\phi=11.0$ we have $\lambda(analytical)=69.82$ with $\lambda(numeric)=70.2$, and for $\phi=30.0$ we found $\lambda(analytical)=190.4$ with $\lambda(numeric)=191.4$. It is interesting that the simple theory from Eqs. (4.1) and (4.2) works so well for such high values of the flow rate. We found that the analytical predictions given by the linear theory [see Eqs. (3.13), (4.1), and (4.2)] remained valid for all the other cases tried as well. These facts attest that a simple mechanism for pattern selection is operating and valid at least in the entire parameter region where we made calculations.

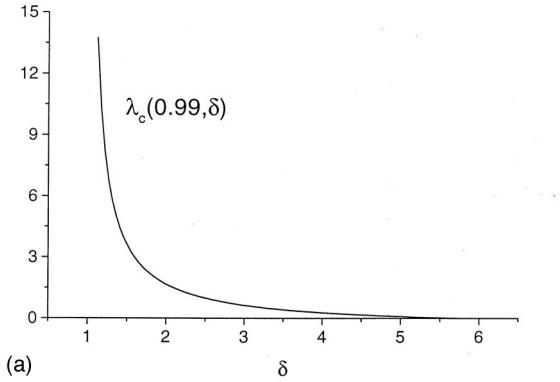


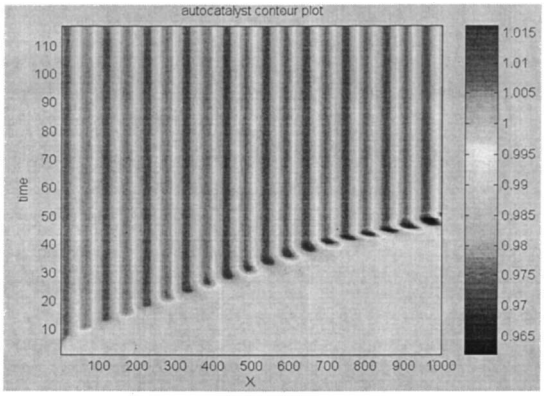


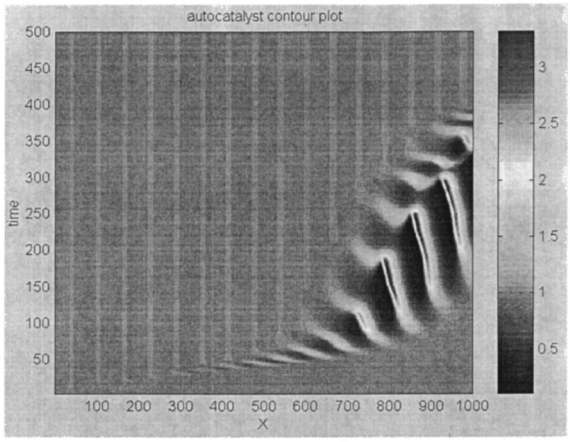


FIG. 3. (a). A plot of the analytically predicted wavelength as given by Eq. (4.2) for $\mu=0.99$ and for $\mu^2=0.9801<\delta<\delta_T=(3+2\sqrt{2})\mu^2=5.71$. (b). Gray scale contour plot of the activator concentration showing the spatial periodic pattern for the case $\delta=1.2$, $\mu=0.99$. Here $\phi_c^*(1.2,0.99)=2.98\ldots$. Here $\phi_{*c}(1.2,0.99)=0$. The wavelength of the periodic pattern is $\lambda(numeric)=20.9$ and we have predicted $\lambda(analytic)=20.822$. (c). Gray scale contour plot of the activator concentration showing the spatial periodic pattern for the case $\delta=2.0$, $\mu=0.99$. Here $\phi_c^*(2.0,0.99)=1.291\ldots$. Here $\phi_{*c}(2.0,0.99)=0$. The wavelength of the periodic pattern $\lambda(numeric)=12.45$ and we have predicted $\lambda(analytic)=12.442$. Note the initial dynamic structure (transient) in the concentration that is eventually washed out from the domain by the flow. A stationary periodic pattern finally invades the entire domain.

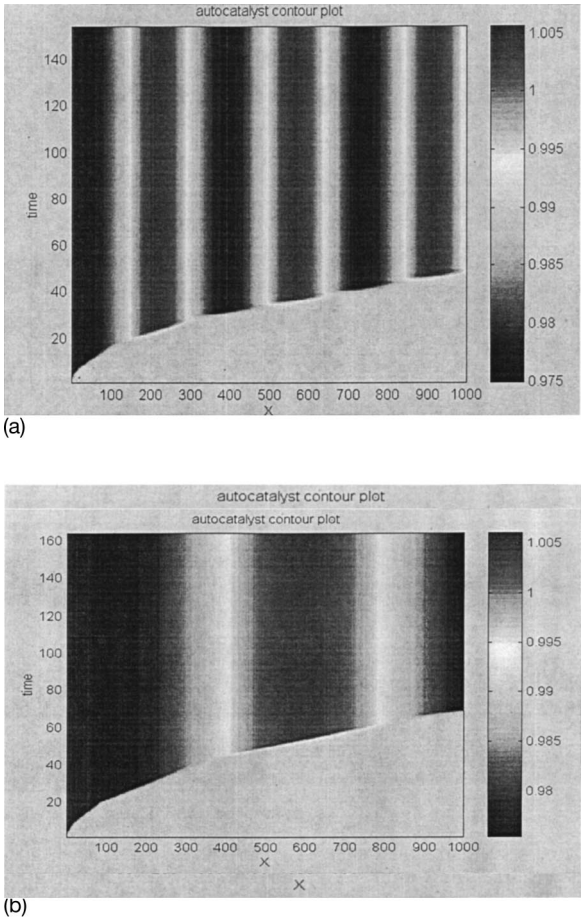


FIG. 4. (a). Gray scale contour plot of the activator concentration showing the spatial periodic pattern for the case when the flow is set away from the critical value: $\delta=1.0$, $\mu=0.99$, $\phi=11.0$. Here $\phi_c^*(1.0,0.99)=9.924$. (b). Gray scale contour plot of the activator concentration showing the spatial periodic pattern for the case $\delta=1.0$, $\mu=0.99$, $\phi=30.0$. Note the increase in the pattern wavelength with the flow as compared to that in Fig. (a).

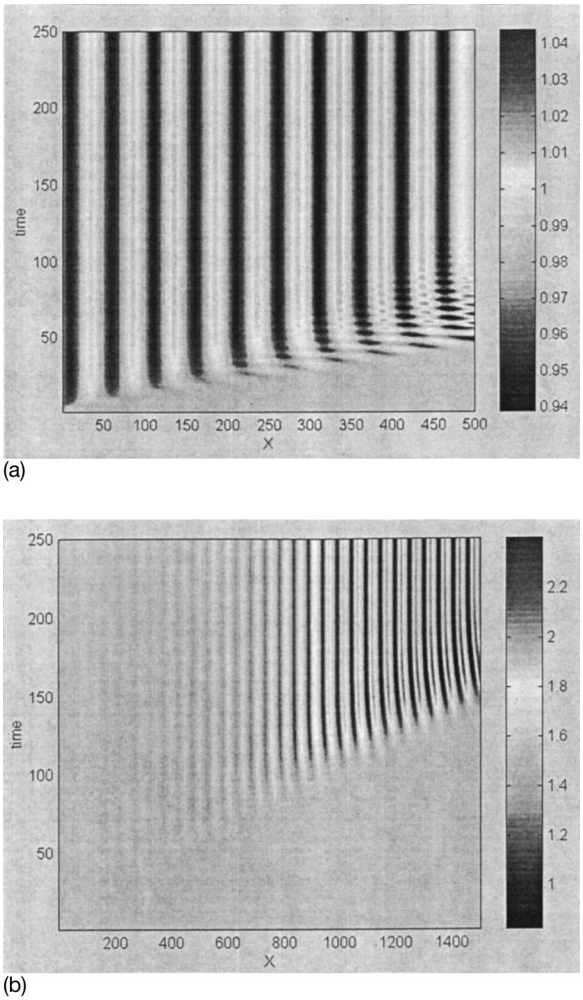


FIG. 5. (a). Gray scale contour plot for the activator species concentration $b$ for the case $\delta=4.5$, $\mu=0.98$, $\phi=0.39$. Here $\phi_{*c}(4.5,0.98)=0.365$. (b). Gray scale contour plot for the autocatalyst concentration for the case $\delta=9.26$, $\mu=1.5$, $\phi=0.55$. Here $\phi_{*c}(9.26,1.5)=0.5035$.

More interesting behavior was seen for values of $\delta$ close to the Turing value $\delta_T$ given by Eq. (3.14). Take, for example, the case $\delta=4.5$, $\mu=0.98$, $\phi=0.39$ (here we have $\delta_T=5.59$). Figure 5(a) displays a color contour plot of the autocatalyst concentration for this case up to the moment when a stationary structure (space-periodic) has been well developed in the full computational domain. We can see that there is an initial transient period during which there is a dynamic competition between two effects: the stationary predicted pattern and a time-depending solution. Eventually the stationary structure dominates for all times. In Fig. 5(b) we show the behavior found for the case $\delta=9.26$, $\mu=1.5$, $\phi=0.55$ for which $\delta_T=13.11$. We see that we do have a stationary pattern but with a more complicated structure. Its front part has higher amplitude than the section near the initial perturbation boundary.

## V. CONCLUSIONS

The Turing mechanism [4] is the textbook example of stationary spatial pattern formation arising in reaction-diffusion systems through the interplay of activator/inhibitor kinetics with fast inhibitor diffusion. The generalization to differential convections of activator and inhibitor species led to the differential-flow instability [3]. The essential novelties of the FDO mechanism lie in the fact that, in its simplest manifestation, i.e., when diffusion is neglected, it is purely kinematic in that it produces stationary waves without requiring any differential transport. Instead, the flow distributes a bulk oscillation through space while the phase at the upstream boundary of the flow determines the phases in the entire flow domain. Fixed boundary conditions at the inflow give rise to stationary waves [1,5] and oscillatory boundary conditions lead to traveling waves [1,15].

The conditions for FDO waves are essentially kinematic, less restrictive, and hence more general than those of the classical differential transport generated patterns (for example, Turing or DIFI) [6,16]. But it is conceivable that in natural and experimental settings, FDO may also be accompanied by differential transport. Possible examples may involve the flow of groundwater through soil or the flow of intracellular constitutive liquids through biological tissues or structures [16,17]. With this type of physical setting in mind we chose the ionic version of the chemical oscillator model of Gray and Scott, generated differential diffusion and flow

by imposing an external electric field, unfolded the FDS stability analysis into the differential diffusion and flow domains, and studied the interfaces of the FDS with the Turing and DIFI domains.

Differential transport was found to add a pronounced dynamical component to the zero-order kinematic FDO model [5]. While the latter predicts FDO waves only when the system oscillates autonomously, differential diffusion and flow expand the range of existence of FDO waves to FDS accompanied by a bigger parameter domain of the kinetic parameter $\mu$, extending to either side beyond the Hopf domain. FDS persists over the whole range of the differential transport ratio $\delta$ up to the Turing limit $\delta=\delta_T$, beyond which Turing patterns are advected by the flow. Thus we conclude that the FDS mechanism is a very flexible one.

In conclusion, we have described a general mechanism that leads to stationary space-periodic structures for a wide range of parameter values and that is distinct from the Turing mechanism. We have pointed out its relation to the classical DIFI and Turing instability regimes: stationary FDS solutions exist only within the convective (DIFI) regime and for a finite range of values of the diffusion ratio $\delta$ up to, and linking with, the Turing regime. Since the conditions of the FDS/FDO mechanisms are easy to implement in the laboratory [5], we envisage that they will play important roles in physical, technological, and biological settings.

## ACKNOWLEDGMENTS

R.A.S. acknowledges financial support from the joint BBSRC/EPSRC Initiative in ''Mathematical Modelling, Simulation and Prediction of Biological Systems,'' Grant No. 43-MMI 09872.

[1] P. Andresen, M. Bache, E. Mosekilde, G. Dewel, and P. Borckmans, Phys. Rev. E **60**, 297 (1999).
[2] S. Kuznetsov, G. Dewel, E. Mosekilde, and P. Borckmans, J. Chem. Phys. **106**, 7609 (1997).
[3] A. B. Rovinsky and M. Menzinger, Phys. Rev. Lett. **70**, 778 (1993).
[4] A. M. Turing, Philos. Trans. R. Soc. London, Ser. B **237**, 37 (1952).
[5] M. Kaern and M. Menzinger, Phys. Rev. E **60**, 3471 (1999).
[6] J. H. Merkin, R. A. Satnoianu, and S. K. Scott (unpublished).
[7] R. Hill, J. H. Merkin, and D. J. Needham, J. Eng. Math. **29**, 413 (1995).
[8] J. H. Merkin, H. Sevcikova, D. Snita, and M. Marek, IMA J. Appl. Math. **60**, 1 (1998).
[9] R. A. Satnoianu, J. H. Merkin, and S. K. Scott, Phys. Rev. E **57**, 3246 (1998).
[10] J. H. Merkin, R. A. Satnoianu, and S. K. Scott, J. Chem. Soc., Faraday Trans. **94**, 1211 (1998).
[11] R. A. Satnoianu, J. H. Merkin, and S. K. Scott, Dynamics and Stability of Systems **14**, 275 (1999).
[12] R. A. Satnoianu, J. H. Merkin, and S. K. Scott, Physica D **124**, 354 (1998).
[13] V. Z. Yakhnin, A. B. Rovinsky, and M. Menzinger, Chem. Eng. Sci. **50**, 2853 (1995).
[14] X. G. Wu, S. Nakata, M. Menzinger, and A. Rovinsky, J. Phys. Chem. **100**, 15 810 (1996).
[15] M. Kaern and M. Menzinger, J. Theor. Biol. (to be published).
[16] J. D. Murray, *Mathematical Biology* (Springer, Berlin, 1989).
[17] A. J. Perumpanani, J. A. Sherratt, and P. K. Maini, IMA J. Appl. Math. **55**, 19 (1995).